analytical chemistry

pubs.acs.org/ac
Article

Vectorial Discrimination of Small Molecules with a Macrocycle Adaptor-Protein Nanopore System and Nanocavity-Dependent, pH Gradient-Controlled Analyte Kinetics

Loredana Mereuta,[#] Adina Cimpanu,[#] Jonggwan Park,[#] Yoonkyung Park,* and Tudor Luchian*

Cite This: *Anal. Chem.* 2025, 97, 5225−5233
Read Online

ABSTRACT: Owing to their intrinsic qualities, protein nanopores became game-changers in the realm of analyte sensing, as they offer an inexpensive and label-free method for sophisticated recognition at the single-molecule level. Here, we exploit the complexation capability of nonfunctionalized γ-cyclodextrin (γ-CD), coupled with its propensity to get reversibly captured inside a wild-type α-hemolysin nanopore (α-HL), and achieve a hybrid construct endowing specific sensing of selected, 5 bases-long oligonucleotides. We find that the molecular discrimination capability of the system has a vectorial-like sensitivity and is influenced by the sidedness and geometry of γ-CD. We showcase that asymmetrical pH changes across the γ-CD-α-HL hybrid and the ensuing electro-osmotic flow offer a simple yet powerful method to control γ-CD capture and residence time inside the nanopore, highlighting the capability of programmable sensing of spatially separated analytes. Unexpectedly, the electro-osmotic flow ensued via pH changes exerted a negligible effect on host (γ-CD)−guest (analyte) interactions, suggesting the complexity arising from a combination of hydrodynamic effects in a restricted environment and electrostatics screening in hydrophobic nanoconfinement. We present evidence that the asymmetric, low pH-mediated, electro-osmotic stabilization of a γ-CD molecule inside α-HL enables probing of β-lactam antibiotic azlocillin encapsulation inside γ-CD under distinct ionization states.

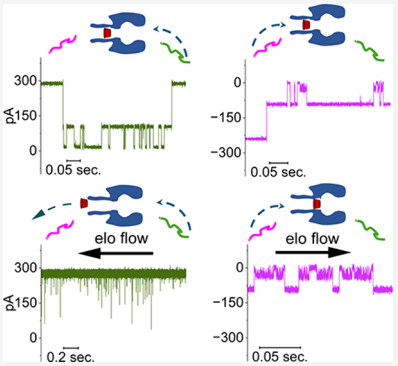

INTRODUCTION

To meet the technological and scientific challenges of detecting, monitoring, and mapping in a low-cost and fast manner, various chemical or physical transformations, nanopore-based approaches evolved as remarkable single-molecule reporters for the task. As a working principle, the reversible interactions of analytes with nanometer-sized cavities isolated in a phospholipid-based insulating membrane, clamped at various electric potentials, alter their conductive properties, which are seen as the emergence of subconductance levels. The frequency and dwell-time values of such levels along with their measured electrical conductance, usually provide direct information on the concentration, size, shape, conformational, or chemical nature of the studied analyte.[1−4]

As an impactful societal application based on this approach and starting with a seminal study that appeared in the late 1990s,[5] the nanopore sequencing paradigm has advanced at an unprecedented fast speed, becoming a valuable tool for real-time and label-free, single-molecule nucleic acid sequencing.[6−8]

While an α-hemolysin (α-HL) nanopore, which is a large heptameric protein pore-forming toxin from *Staphylococcus aureus*, has been the first widely used nanopore in the nanopore research community,[5,8,9] there is currently a large diversity of nanopore-forming proteins, including *Mycobacterium smegmatis* porin A (MspA),[10] aerolysin,[11,12] Fragaceatoxin C (FraC),[13] or CsgG:CsgF,[14] to name just a selected few.

Contemporarily, protein nanopores are among key components permitting label-free detection and analysis at the single molecule level of structural information in peptides and proteins,[15−20] oligo- and polysaccharide sequences,[21] and measurement of molecular forces[22,23] and became increasingly useful in forensic analysis[24] or medical diagnosis concerning various pathologies.[25,26]

Despite all proven qualities, challenges still plague accurate nanopore-based molecular characterization, most commonly affected by the relatively small size with respect to the nanopore inner cavity of the studied analytes and fast translocation rates. To address these, a rich variety of studies have demonstrated that the translocation process is influenced and can be tuned by the nanopore geometry and chemical composition,[27] site-directed mutagenesis on the nanopore,[28−30] and electrolyte properties such as viscosity, salt concentration, pH, or temperature.[31−36] In recent years,

Received: December 15, 2024
Revised: February 8, 2025
Accepted: February 13, 2025
Published: February 28, 2025

https://doi.org/10.1021/acs.analchem.4c06801
Anal. Chem. 2025, 97, 5225−5233

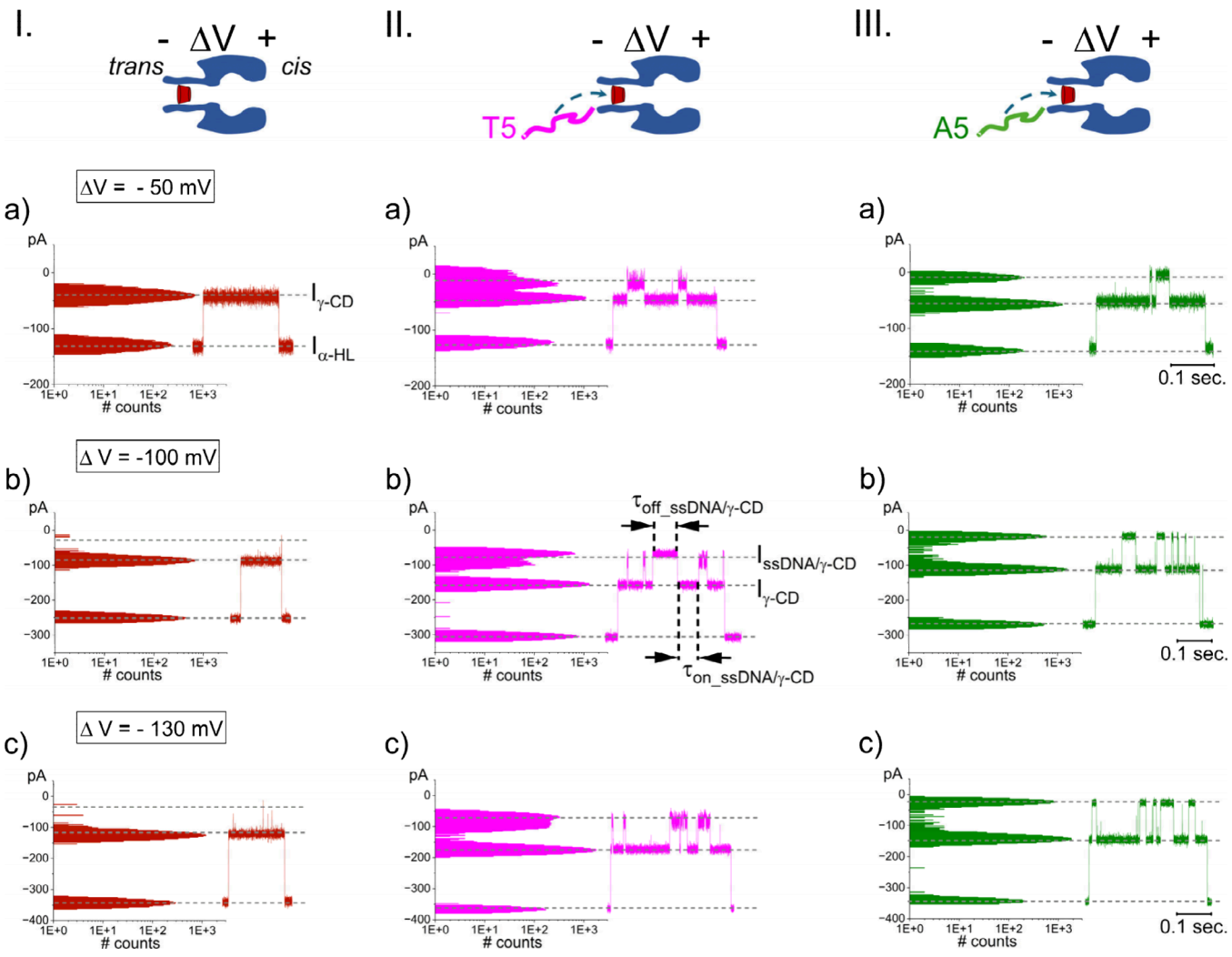

Figure 1. Reversible capture of trans-added T5 and A5 fragments by a γ-CD-α-HL system. I. (a−c) Selected traces and corresponding all-point histograms showing the reversible formation of a γ-CD-α-HL at different trans-negative transmembrane voltages (ΔV), seen as ionic current excursions from $I_{\alpha\text{-HL}}$ to $I_{\gamma\text{-CD}}$. Capture of the trans-side added T5 (II, a−c) or A5 fragments (III, a−c) [16 μM] generates supplementary blockades of the ionic current measured through the γ-CD-α-HL, to the $I_{\text{ssDNA}/\gamma\text{-CD}}$ level. For brevity, we represent the γ-CD as a truncated cone, and A5 and T5 fragments are represented in green and magenta, respectively. In this experiment and throughout the manuscript, unless noted otherwise, the aqueous concentration of γ-CD was 40 μM, [KCl] = 3 M, and the electrolyte was buffered at pH = 7.1 with 10 mM HEPES.

numerous studies have also highlighted the influence of the electro-osmotic flow on analyte capture and translocation processes across nanopores.[37−48]

In many cases, the signal-to-noise resolution of translocation events generated by small molecules remains insufficient and precludes accurate identification. To alleviate this, hybrid constructs were tested by using host molecules lodged within the α-HL pore, including cyclodextrin,[49−54] cyclic peptide,[55] or cucurbituril,[56] to serve as nanoreactors with even lower dimensions than the nanopore itself, engage in reversible host−guest interactions and allow the investigation in finer details of single-molecule blockade events, thus improving sensing and characterization. As in most of these examples, site-directed protein mutagenesis and chemically modified cyclodextrins (CDs) were prerequisites for implementing the detection protocol; technical challenges certainly arise for nonexpert nanopore users and thus prevent wider field applications of the approach.

Here we employ a neutral γ-cyclodextrin (γ-CD) adapter and demonstrate that the hybrid (γ-CD-α-HL) system can distinguish between adenine (A) and thymine (T) nucleotides in 5-mers homopolymers (denoted herein by A5 and T5). We show that the detection and identification of A5 and T5 can be performed concurrently with both analytes added separately on cis and trans sides of the γ-CD-α-HL. Unexpectedly, we found that while both fragments traverse the γ-CD-α-HL system, the "molecular fingerprint" indicative of single-molecule identification of A5 and T5 fragments inside the γ-CD-α-HL depends upon the capture geometry, i.e., from the primary or secondary face of γ-CD.

We discovered that an electro-osmotic flow generated in real-time by asymmetrical pH changes across the hybrid nanopore entraps a γ-CD molecule inside the α-HL for ∼seconds, without the use of covalent chemistry or other immobilization techniques, or it can reversibly exclude the γ-CD from lodging inside the α-HL.

Finally, we leveraged the electro-osmotic flow-induced prolongation of the γ-CD inside the wild-type α-HL, and revealed the pH-dependent interaction of a monoanionic β-

https://doi.org/10.1021/acs.analchem.4c06801
Anal. Chem. 2025, 97, 5225−5233

lactam antibiotic (azlocillin) with the γ-CD-α-HL system at the single-molecule level.

MATERIALS AND METHOD

Reagents used and sample preparation are fully reported in the Supporting Information. The electrophysiology experiments were performed as previously reported.[23,30] The recording electrolyte contained 3 M KCl buffered with 10 mM HEPES (pH = 7). To attain pH changes from neutral to acidic values during the same experiment, HCl was added in a dropwise manner from a stock solution. Depending on the experiment, ssDNA fragments were pipetted on the cis or trans side of the α-HL nanopore and inserted into the lipid membrane. Ionic currents were recorded with an Axopatch 200B or Multiclamp 700B amplifier (Molecular Devices, USA) in the voltage-clamp mode, and the electrical signals were digitized at a sampling frequency of 50 kHz with a NI PCI 6221 16-bit acquisition board (National Instruments, USA) and low-pass filtered at 10 or 12 kHz. Alternatively, we employed for data recording and analysis the ePatch amplifier (ELEMENTS SRL, Italy).

RESULTS AND DISCUSSION

Selective, Single-Molecule Detection of Adenine (A5) and Thymine (T5) Fragments with the Hybrid γ-CD-α-HL System. The reason behind focusing on A5 and T5 fragments was 2-fold: (i) first, we sought to endow technical simplicity and feasibility on the approach, as these homopolymers were expected to produce a visible blockade fingerprint; (ii) second, the volume difference between these fragments is small enough as to challenge the detection system with regard to its ability to distinguish closely related analytes, based on steric considerations alone.

In the first series of experiments, analyte sensing was achieved by interacting a single wild-type α-HL nanopore with a nonfunctionalized γ-CD molecule, added on the trans side of the lipid membrane that was hosting the nanopore and subjected to a potential difference (ΔV). The external diameters of γ-CD's primary and secondary face are 1.61 and 1.69 nm, respectively,[57] allowing it to enter from the ∼2.4 nm in diameter trans side opening of α-HL, yet unable to pass through the narrowest region (∼1.4 nm in diameter) of the nanopore.

As presented in Figure 1, the reversible capture of a single γ-CD by the nanopore at trans-negative ΔVs was quantified via the partial alterations of the ionic current from the open nanopore value $I_{\alpha\text{-HL}}$ to $I_{\gamma\text{-CD}}$ (Figure 1, I, a−c). The subsequent electrophoretic capture of trans-added A5 or T5 fragments by the γ-CD-α-HL complex generated reproducible blockades seen as upward alteration in the measured ionic current from $I_{\gamma\text{-CD}}$ to almost full obstruction ($I_{\text{ssDNA}/\gamma\text{-CD}}$) (Figure 1, II, III, a−c), reflecting the signatures of the host (γ-CD)−guest (T5 or A5) interactions.

Similar blockades were observed with the A5 and T5 added on the cis side of the membrane (Figure S1), demonstrating that a γ-CD entrapped inside the α-HL is accessible from either its primary or secondary side. As displayed in Figures 1 and S1, to quantify the reversible capture of either A5 or T5 ssDNA by a γ-CD immobilized inside the nanopore, three descriptors were employed: the association ($\tau_{\text{on\_ssDNA}/\gamma\text{-CD}}$) and dissociation time intervals ($\tau_{\text{off\_ssDNA}/\gamma\text{-CD}}$) and the blockade extent quantified as $\Delta I_{\text{ssDNA}/\gamma\text{-CD}} = I_{\text{ssDNA}/\gamma\text{-CD}} - I_{\gamma\text{-CD}}$.

Supplementary experiments undertaken with A5 added at distinct concentrations on either the cis or trans side of the nanopore revealed that during each γ-CD capture event, the average of $\tau_{\text{off\_A5}/\gamma\text{-CD}}$ time intervals was practically invariant versus A5 concentration, whereas the average of $\tau_{\text{on\_A5}/\gamma\text{-CD}}$ time intervals measured between A5-induced successive blockade events decreased linearly with the increase in A5 concentration, all suggestive of a bimolecular A5-γ-CD interaction (Figure S2).

Unlike the situation in which either the A5 or T5 fragment was captured from the cis side (Figure S1, II, III), when the T5 entered the γ-CD from the trans side, and upon encapsulation, a clear set of sub-blockade events were elicited before fragment escape, and this is represented by the double peak-like appearance of the ionic current level assigned to the most obstructed state in the all-point histograms (Figure 1, II). This behavior was absent in the case of A5-γ-CD interactions (Figure 1, III), further evidenced in Figure S3. This is an interesting finding, from a 2-fold perspective: (i) the γ-CD-α-HL complex enables distinguishing between two such length-similar fragments, T5 and A5, not necessarily through the blockade extent (*vide infra*), but the emergence of additional current fluctuations reflecting the dynamics of fragments captured inside the γ-CD; (ii) this phenomenon bears a vectorial-like propensity, as it is side-specific with respect to analyte capture inside the γ-CD. We posit that this is an indirect indication that a γ-CD molecule entrapped inside the α-HL exposes its secondary face toward the β-barrel entrance (trans side) of the nanopore. In this configuration and due to thermal fluctuations, the slightly lower in volume, entrapped T5 fragment, is able to probe multiple times the rim of the γ-CD's primary face while adjusting its orientation for enhanced contact with the γ-CD, reflected by the subconductance fluctuations seen in Figure S3b, enlarged trace, before escaping on the opposite side.

Due to the stochastic nature of such capture processes, ssDNA-α-HL interactions do occur while the nanopore is devoid of γ-CD inclusion. However, since the effective inner volume of the γ-CD-α-HL complex is smaller than that of the α-HL alone, control experiments illustrated in Figure S4 demonstrate that the electric signature of such concurrent processes, i.e., the ssDNA blockade of either γ-CD-α-H or α-HL alone, is discernible in either case.

Interaction of A5 and T5 Fragments with the γ-CD-α-HL Complex is Voltage-Dependent. To examine the interaction landscape between the A5 and T5 fragments and the γ-CD immobilized inside the α-HL, we carried out experiments with the analytes added on either side of the nanopore at a fixed concentration but under variable ΔVs. Subsequent quantitative analysis of these interactions was implemented through statistical evaluation of blockade values ($\Delta I_{\text{ssDNA}/\gamma\text{-CD}}$) and dwell-time distributions. Dwell-time histograms of the association ($\tau_{\text{on\_ssDNA}/\gamma\text{-CD}}$) and dissociation time intervals ($\tau_{\text{off\_ssDNA}/\gamma\text{-CD}}$) of either fragment interacting with the γ-CD-α-HL were constructed, and each was fit to a single exponential (data not shown) to obtain the mean association and dissociation time values (Figure S5).

As indicated by the decrease of both ($\tau_{\text{on\_ssDNA}/\gamma\text{-CD}}$) and ($\tau_{\text{off\_ssDNA}/\gamma\text{-CD}}$) mean time values with the increase of the ΔV in either experimental configuration, i.e., T5 and A5 added on the cis (Figure S5, I, a,b) or trans side (Figure S5, II, a,b), it was concluded that both fragments traverse across the γ-CD-α-HL, whereby the confined γ-CD nanocavity induces an

https://doi.org/10.1021/acs.analchem.4c06801
Anal. Chem. 2025, 97, 5225−5233

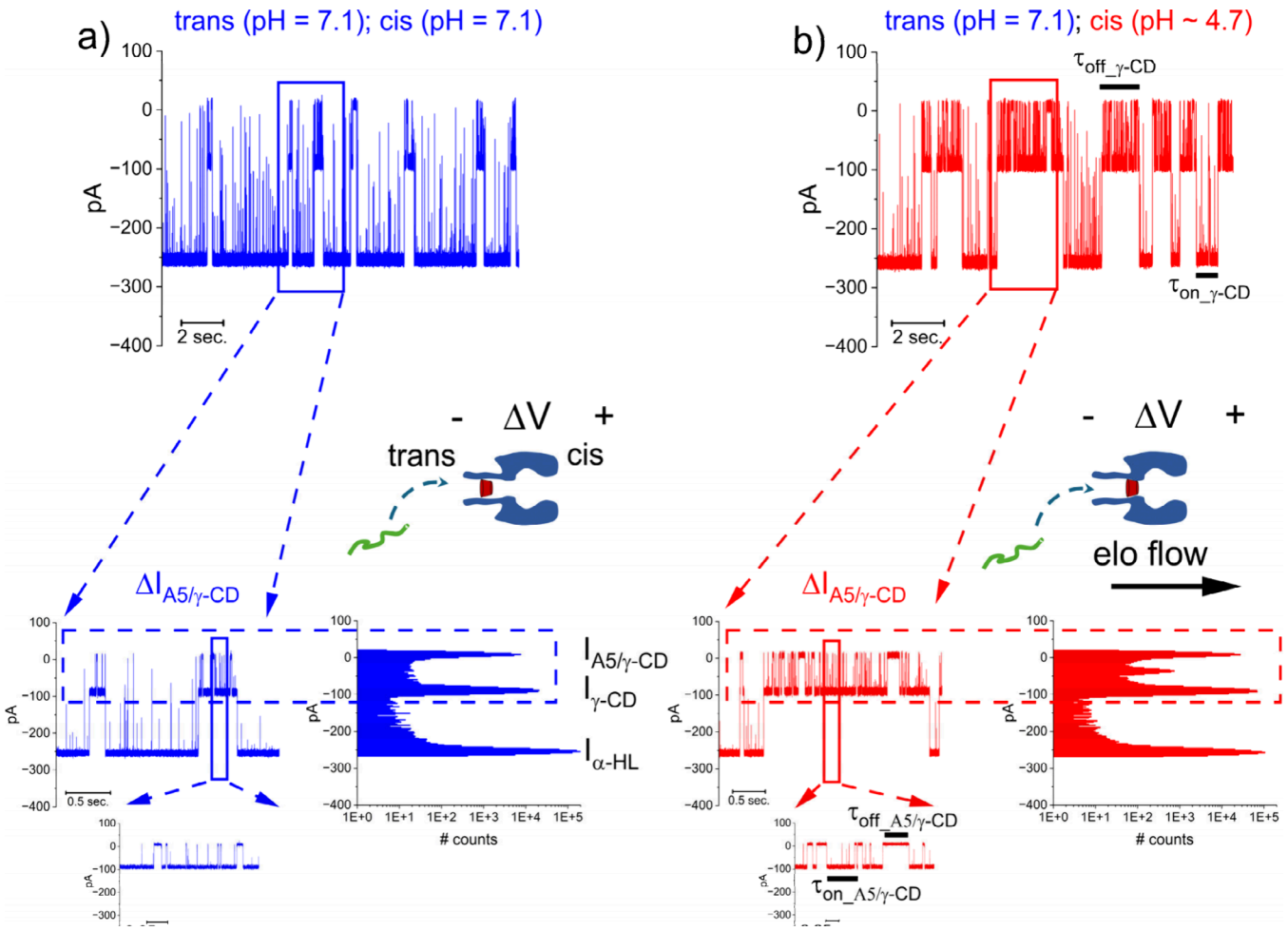

Figure 2. Asymmetric pH changes across the nanopore generate more stable γ-CD-α-HL systems. Representative traces excerpted from the same experiment produced by trans-added A5 [16 μM] interacting reversibly with a γ-CD-α-HL at $\Delta V = -100$ mV, when at pH = 7.1, in both cis and trans sides of the nanopore (a) and following a change of the pH to ~4.7 in the cis side only (b). The enlarged traces beneath each recording in a and b illustrate clearly the reversible A5-γ-CD interactions inside the α-HL, characterized by the dissociation ($\tau_{off\_A5/\gamma\text{-CD}}$) and association ($\tau_{on\_A5/\gamma\text{-CD}}$) time intervals. The accompanying all-point histograms illustrate the blockade events indicative of the A5-γ-CD interactions, and the dashed rectangles isolate representative A5-induced blockade events within the γ-CD-α-HL, quantified via $\Delta I_{A5/\gamma\text{-CD}}$.

unstacked, linear conformation of fragments, facilitating their passage.

We also quantified the voltage-dependent current blockade ($\Delta I_{ssDNA/\gamma\text{-CD}}$) induced by the host−guest interaction of γ-CD-α-HL with either T5 or A5 added on the cis (Figure S5, I, c) or trans side (Figure S5, II, c). The linear dependence of the blockade extent vs ΔV indicates that the shape of the unstacked fragments remains invariant during translocation at various potentials, with no conformer intermediates. This is also substantiated by the approximately constant values of the relative blockade extents calculated while a guest fragment (T5 or A5) resides in the cavity of a γ-CD, defined as $\frac{\Delta I_{ssDNA/\gamma\text{-CD}}}{I_{\gamma\text{-CD}}}$ (Table S1).

Serendipitously, data presented in Figure S5, I, c and II, c reveal that host (γ-CD)−guest (A5 or T5) interactions, distinguish most clearly between the guest types when they enter the α-HL-residing γ-CD from the trans side (see also Table S1). We point out that in such evaluations, the value for $I_{T5/\gamma\text{-CD}}$ used to calculate $\Delta I_{T5/\gamma\text{-CD}} = I_{T5/\gamma\text{-CD}} - I_{\gamma\text{-CD}}$ and eventually compared to the current reductions entailed by the A5 fragment under similar conditions ($\Delta I_{A5/\gamma\text{-CD}} = I_{A5/\gamma\text{-CD}} - I_{\gamma\text{-CD}}$), was an average over the sub-blockade events elicited while T5 fragments obstruct to the largest extent the γ-CD, seen also as a double peak-like appearance of the $I_{T5/\gamma\text{-CD}}$ level in Figure 1, II, a−c and Figure S3b.

Subsequently, we estimated the volume of the γ-CD-encapsulated, trans-added T5 or A5 fragments. While the inner topology of the γ-CD departs from cylinder-like and resembles a truncated cone, and knowing that in such situations the ionic current blockade extent varies with the analyte's axial position inside the host molecule,[58] we simplified our calculations and modeled the γ-CD nanocavity as a cylinder with an average diameter of 0.86 nm and volume of $v_{\gamma\text{-CD}} = 0.45$ nm^3. By using data reported in Table S1, it follows that the estimated volume of the T5 and A5 fragments viewed as cylinders, from recordings undertaken at $\Delta V = -100$ mV and neglecting the access resistance to the host (γ-CD), were $\delta_{ssDNA} = \frac{\Delta I_{ssDNA/\gamma\text{-CD}}}{I_{\gamma\text{-CD}}} v_{\gamma\text{-CD}} = 0.38$ nm^3 for the A5 fragment and 0.25 nm^3 for the T5 fragment. By comparing these results with the data sets presented in literature, which indicate volumes of 0.32 nm^3 for single A nucleotides and 0.31 nm^3 for single T nucleotides,[59] the immediate conclusion is that the host (γ-CD)−guest (A5 or T5) blockades correspond to single

https://doi.org/10.1021/acs.analchem.4c06801
Anal. Chem. 2025, 97, 5225−5233

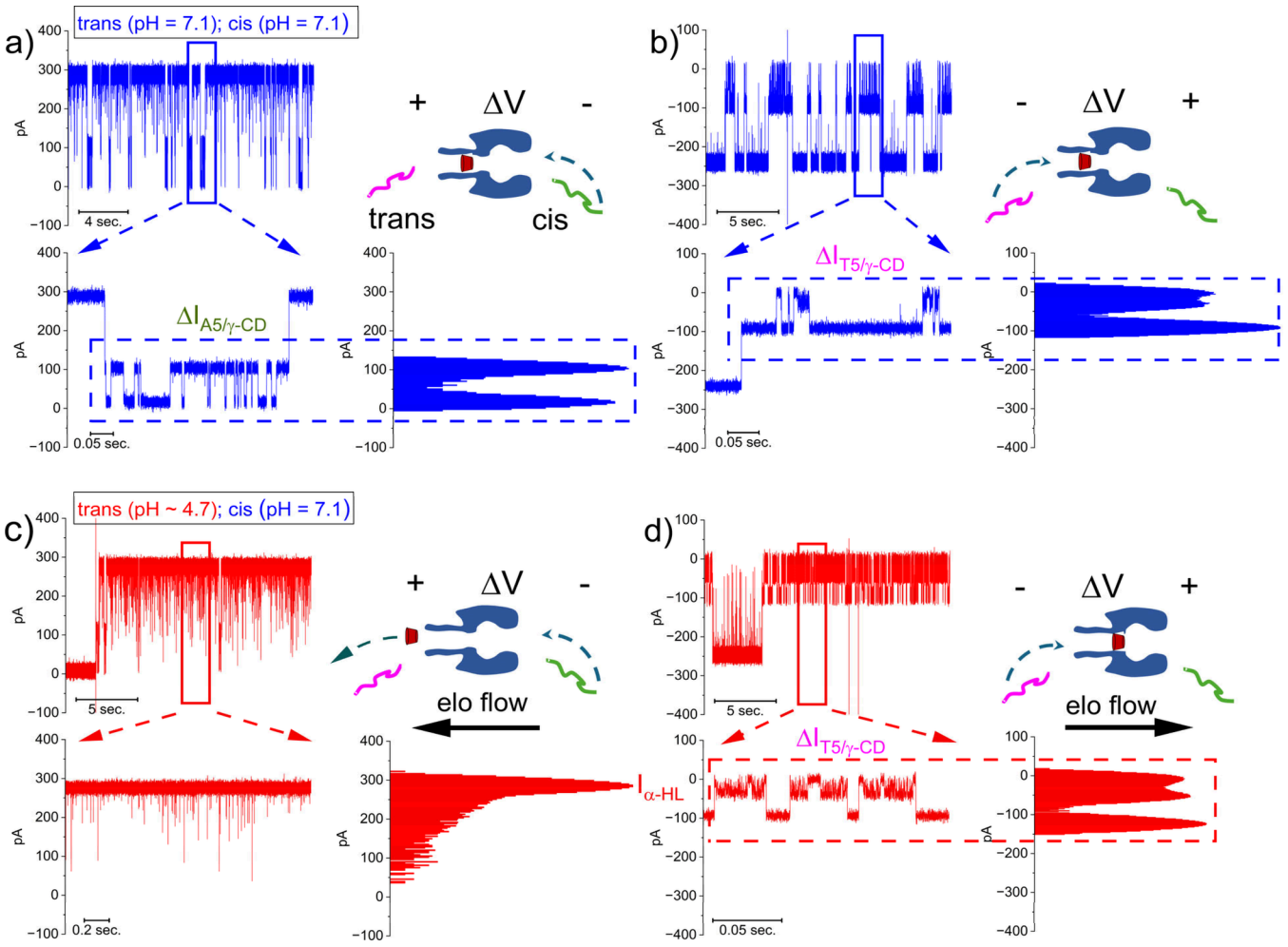

Figure 3. Electro-osmotic flow dominates γ-CD capture inside the α-HL and endows Δ*V* sign-dependent, programmable analyte detection. Around neutral pH, spatially separated A5 (cis side) and T5 (trans side) fragments [16 μM] are disjointly captured by an electrophoretic force and detected with the γ-CD-α-HL by the simple change of the Δ*V* polarity of A5 at +100 mV (a) and T5 at −100 mV (b). Subsequent change of the pH to ∼4.7 in the trans side only generates a dominant electro-osmotic flow that, depending on the Δ*V* polarity, is either cis → trans (at +100 mV, c) or trans → cis (at −100 mV, d) oriented, leading to the total exclusion of the γ-CD molecule from the α-HL (c) and programmable detection of T5-γ-CD interactions only (d). The presented all-point histograms in a, b, and d illustrate the conductance states ($\Delta I_{\text{T5 or A5}/\gamma\text{-CD}}$) ensued by analyte (A5 or T5)-γ-CD-α-HL interactions, as highlighted by the dashed rectangles.

nucleotides from either fragment temporarily lodged inside the γ-CD during translocation.

From a kinetic perspective, the capture inside and translocation across the γ-CD-α-HL occurs slower for the T5 as compared to the A5 fragment, and this is more obvious with the trans-added A5 and T5 (Figure S5, II, a,b). This is a counterintuitive result, given at the very least the slightly less voluminous T5 vs A5, which renders electric mobility of the former correspondingly higher. Above results indicate that while the α-HL-entrapped γ-CD facilitates quantitative sensing at the single-molecule level of very similar A5 and T5 fragments in terms of electrical charge and size, the spatial interactions between analytes and the γ-CD's internal environment dictate in a nontrivial manner the detection fingerprint.

Electro-osmotic Influence on γ-CD-α-HL Interactions and Molecular Transport across γ-CD-α-HL. To offer a reasonable argument for the insertion of charge neutral cyclodextrins into the α-HL, electro-osmotic flow was proposed as the main driving force, and experiments established that the binding site for β-CD lies in the vicinity of Met-113.[43,60] To the end of achieving γ-CD-α-HL constructs likely useful as cheap and easy-to-use components of stochastic sensors, we built up a simpler strategy for lengthening the residence times of γ-CD inside the α-HL. In a simple embodiment, we set to probe the hypothesis that asymmetrically imposed, low pH-mediated electro-osmosis (elo)[30] is capable of retaining more effectively a neutral γ-CD molecule inside the nanopore.

Figure 2 is representative for a set of experiments demonstrating that when pH is lowered asymmetrical to the cis side only, from a neutral (pH = 7.1) to a slightly acidic value (pH ∼ 4.7), the averaged residence time of a γ-CD inside the α-HL ($\tau_{\text{off\_}\gamma\text{-CD}}$) increases while its averaged capture time ($\tau_{\text{on\_}\gamma\text{-CD}}$) decreases (see also Table S2). This led us to conclude that the cis-side, low-pH-augmented electro-osmotic flow, which is trans → cis oriented on the negatively biased nanopore, as displayed in Figure 2, acts as an efficient mechanism to entrap individual γ-CD molecules.

Supplementary experiments revealed that by further lowering the pH in the cis side ($pH_{cis} \sim 3$; $pH_{trans} = 7.1$) or both sides of the nanopore ($pH_{cis} \sim 3$; $pH_{trans} \sim 3$), and otherwise similar conditions as above, a more pronounced effect of the

https://doi.org/10.1021/acs.analchem.4c06801
Anal. Chem. 2025, 97, 5225−5233

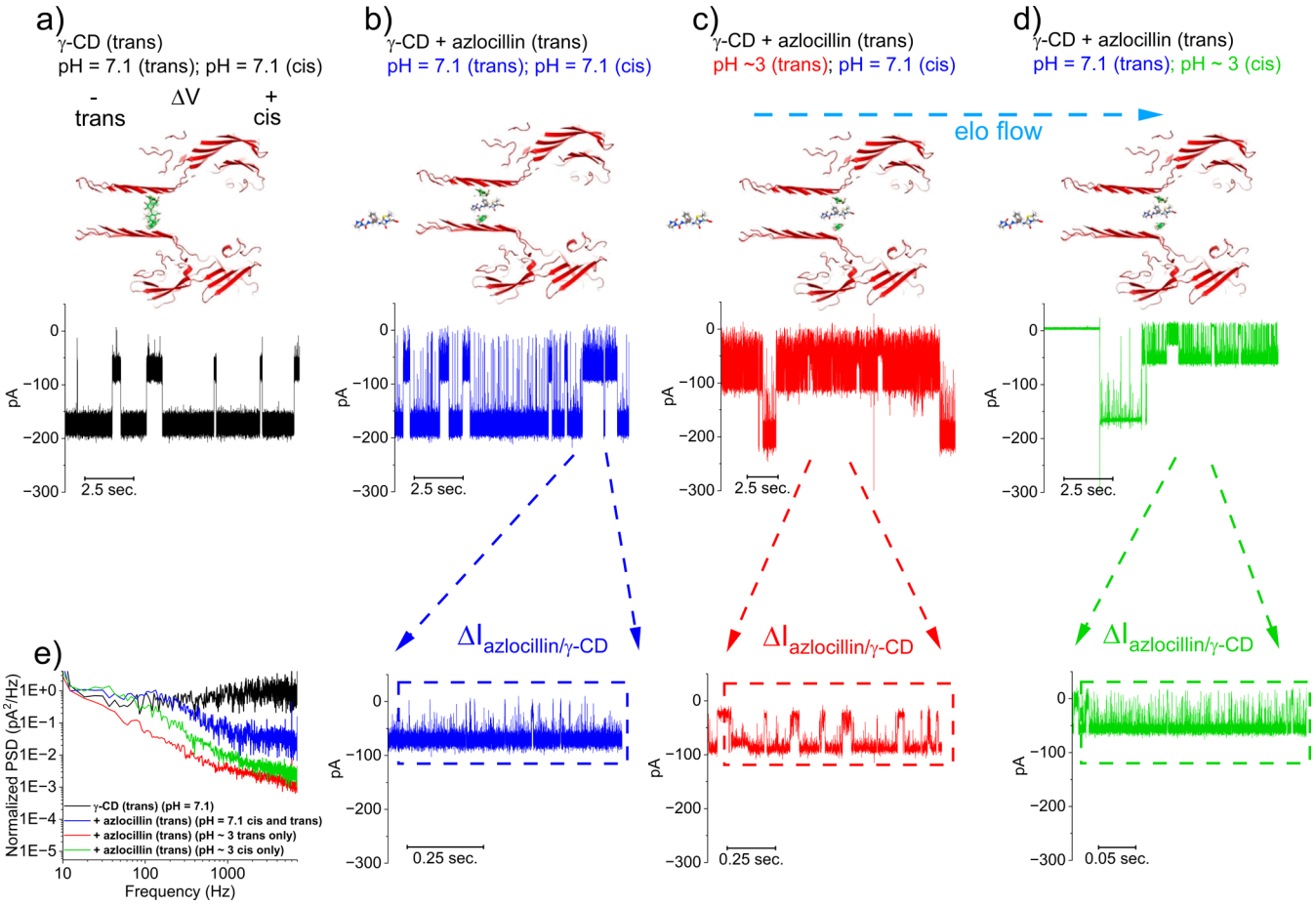

Figure 4. Hooking two fish with a single bait: an asymmetrically induced pH gradient permits a longer examination of azlocilin-γ-CD interactions while also changing the analyte's ionization state. Selected traces recorded at $\Delta V = -70$ mV in symmetrical neutral pH, showing that, unlike the case of the analyte-free γ-CD-α-HL system (a), the capture of trans-side added azlocillin generates ionic current fluctuations ($\Delta I_{\text{azlocillin}/\gamma\text{-CD}} = I_{\text{azlocillin}/\gamma\text{-CD}} - I_{\gamma\text{-CD}}$) (b) (see also the enlarged trace excerpt beneath panel b). (c) Asymmetrical pH modification (pH ~ 3 trans; pH = 7.1 cis) lowers the charge of trans-added azlocillin, generates an electro-osmotic flow (elo) leading to a more stable γ-CD-α-HL complex, and visibly alters the kinetics of azlocillin-γ-CD-α-HL interactions (see the enlarged trace beneath panel c). (d) The reversed asymmetrical pH modification (pH = 7 trans; pH ~ 3 cis) leaves the trans-added azlocillin charge virtually unchanged, yet it permits the generation of an electro-osmotic flow augmenting the stability of the γ-CD-α-HL complex (see also enlarged trace beneath panel d). (e) Normalized power-spectrum density (PSD) traces quantifying the ionic current fluctuations illustrative of a captured γ-CD inside the α-HL at neutral pH (γ-CD, black trace) and pH-dependent azlocillin-γ-CD interactions. The α-HL and an entrapped γ-CD, seen on the sagittal section, were drawn to scale. The molecular representation of azlocillin (panels b–d) is not drawn to scale.

electro-osmotic flow on the γ-CD capture inside the α-HL is entailed (see Figure S6 and Table S3).

To supplement these findings, we carried out experiments under similar conditions to those presented above, except that the pH alteration was induced in the trans side of the nanopore. To mitigate low pH-induced alterations on the protonation of trans-added A5 fragments, we restricted the study to pH ~ 4.7. Under such conditions, and as predicted by the Henderson–Hasselbalch equation, the partial protonation of adenine ($pK_a \sim 3.6$) bases add only $\sim +0.36|e^-|$ as a bare contribution to the net charge of A5 fragments, whose phosphate groups protonation state ($pK_a \sim 1$) remains largely unchanged (net charge of $\sim -1|e^-|$ per phosphate). Representative data derived from such experiments (Figure S7) and statistical analysis (Table S2) revealed an even more pronounced effect of the electro-osmotic flow manifested especially on the γ-CD capture kinetics. We suggest that by lowering the pH in the trans as opposed to the cis side of the nanopore, the more effective protonation of the D127 and D128 amino acids from each monomer forming the β-barrel entrance of the heptameric α-HL on the trans side produces a larger electro-osmotic flow in the former as compared to the latter case.

We extended the statistical analysis of data displayed representatively by Figure 2 and Figure S7 to assess the effect of the asymmetrically (cis or trans) lowering, pH-induced, trans → cis oriented electro-osmotic flow on the reversible capture of trans-added A5 fragments by the γ-CD ($\tau_{\text{on\_A5}/\gamma\text{-CD}}$) and its release from the γ-CD's interior ($\tau_{\text{off\_A5}/\gamma\text{-CD}}$) (see Figure 2b, the enlarged trace, for a better view on how such intervals were represented). The synthetic results are shown in Table S2. Interestingly, the reversible A5-γ-CD interactions (quantified through the average values $\tau_{\text{off\_A5}/\gamma\text{-CD}}$ and $\tau_{\text{on\_A5}/\gamma\text{-CD}}$) do not appear to be dramatically affected by the electro-osmotic flow in either context (i.e., pH lowered in the cis or trans sides of the protein). This is an unexpected discovery, as a naïve thinking one would have expected a similar influence of the electro-osmotic flow on the A5-γ-CD interactions, as for the case of the γ-CD-α-HL reversible capture. Further simulations and experiments are needed to

https://doi.org/10.1021/acs.analchem.4c06801
Anal. Chem. 2025, 97, 5225–5233

fully illuminate this phenomenon, which may be indicative of the fact that the limited number of water molecules contained inside the γ-CD (only ∼5 to 12), coupled with its highly hydrophobic interior, impact nontrivially upon the propensity of the electro-osmotic flow to alter analyte trafficking.

Vectorial Effect of the Electro-Osmotic Flow across the α-HL upon Concurrent Probing of Distinct Analytes. By extending the rationale described above, one may argue that the γ-CD may not only be stabilized inside the α-HL through the action of the electro-osmotic flow, but also prevented from the capture inside the nanopore, thus allowing the programmable detection of a given analyte. To probe this, we devised an experiment during which spatially separated A5 and T5 fragments were allowed to interact individually with the γ-CD-α-HL.

Our data demonstrate that at neutral pH and depending upon the polarity of the ΔV, either a cis-added A5 (Figure 3a) or trans-added T5 (Figure 3b) fragment enters the nanopore under the influence of the electrophoretic force and gets captured reversibly by a residing γ-CD. Note that at neutral pH, the anionic selectivity of the α-HL is modest ($\frac{P_{K^+}}{P_{Cl^-}} = 0.86$, around pH = 7.1), so that electro-osmotic flux reversal through switching the ΔV polarity does not prevent γ-CD from entering the nanopore. This scenario changes drastically once the magnitude and orientation of the electro-osmotic flow are altered via pH changes in the bathing electrolyte.

As displayed in Figure 3c,d, the trans-side, real-time pH lowering to ∼4.7 during the same experiment generates an augmented electro-osmotic flow that, depending on its orientation, set simply by the sign of the applied ΔV, stabilizes the γ-CD inside the nanopore (Figure 3d) or completely prevents it from entering it (Figure 3c). Consequently, the sensitive detection of the T5 becomes feasible at $-\Delta V$s, which set a trans → cis oriented electro-osmotic flow, whereas at $+\Delta V$s, the cis → trans oriented electro-osmotic flow precludes the formation of the γ-CD-α-HL complex.

The low pH-mediated exclusion of the γ-CD from the nanopore is fully reversible. As discovered, continuous changes of the electrolyte acidity from pH = 7.1 to pH ∼ 4.7 and then to pH ∼ 10.5 on a positively biased α-HL, determines in the first step γ-CD exclusion from the nanopore and the implicit lack of specific detection of cis-added A5 (Figure S8), followed by recapture of the γ-CD inside the nanopore in the second step, ensuing specific A5 detection (Figure S9). The immediate explanation for this finding is that pH changes from neutral or acidic to alkaline values, known to switch the α-HL ionic selectivity from anionic to cationic,[60] entail the reversal of the electro-osmotic flux orientation across the α-HL nanopore, otherwise maintained at the same transmembrane potential.

Low pH-Dependent, Prolonged γ-CD Residence inside α-HL Facilitates the Investigation of Anionic Azlocillin-γ-CD Interactions. In many practical applications involving drug formulations, cyclodextrins are used as excipients, and various techniques are used to map and test the chemical stability and efficacy of antibiotic−cyclodextrin formulations.[61,62] To further emphasize the applicability of the present work, we showcase the use of electro-osmotic stabilization of a γ-CD inside the α-HL, to reveal the pH-dependent kinetics of γ-CD-azlocillin interactions at the single-molecule level.

At a transmembrane potential of $\Delta V = -70$ mV, the trans-side addition of azlocillin [200 μM] at pH = 7.1 determines vigorous current fluctuations through the γ-CD-α-HL (Figure 4a,b), entailed by the electrophoretic capture of the anionic azlocillin (azlocillin is a weak acid with a pK_a as low as 2.65) inside the γ-CD. By using structural information on azlocillin,[63] we represented it in a simplified view as a cylinder with a length of ∼8.5 Å and a diameter of ∼4.6 Å, thus having a volume of ∼0.14 nm^3. By comparison with the estimated volume of the γ-CD interior ($\upsilon_{\gamma\text{-CD}} = 0.45$ nm^3), we concluded that the ionic current fluctuations ($\Delta I_{azlocillin/\gamma\text{-CD}}$) exemplified in Figure 4b stem from the stochastic passage of a maximum number of three azlocillin molecules across the γ-CD.

To probe the impact of the azlocillin ionization state on its interaction with the γ-CD, we extended the experiment outlined in Figure 4b by imposing the trans side only, pH changes to ∼3, seeking to (i) alter the partial charge on trans-added azlocillin (the Henderson−Hasselbalch equation predicts that at pH ∼ 3, the azlocillin net charge becomes ∼30% lower than that at pH = 7.1) and (ii) generate an electro-osmotic flow, which at $\Delta V = -70$ mV is trans → cis oriented, it helps stabilize a γ-CD molecule inside the α-HL, thus permitting a better inspection of azolicillin-γ-CD interactions.

Following experiments embodied by the trace in Figure 4c, we calculated the relative blockade induced by γ-CD-encapsulated azlocillins on the ionic current ($\Delta I_{azlocillin/\gamma\text{-CD}} = I_{azlocillin/\gamma\text{-CD}} - I_{\gamma\text{-CD}}$) as $\frac{\Delta I_{azlocillin/\gamma\text{-CD}}}{I_{\gamma\text{-CD}}} = 0.7 \pm 0.016$ (mean ± SEM), indicating a blockade volume of $\delta_{azlocillin} = \frac{\Delta I_{azlocillin/\gamma\text{-CD}}}{I_{\gamma\text{-CD}}}\upsilon_{\gamma\text{-CD}} = 0.3 \pm 0.007$ nm^3 (mean ± SEM). By dividing this to the estimated volume of a single azlocillin molecule (∼0.14 nm^3), we arrive at an average number of 2.2 ± 0.05 (mean ± SEM) azlocillin molecules hosted inside the γ-CD. As detailed in the Supporting Information within the framework of Poisson statistics ("Simplified formalism describing the probability of simultaneous analytes capture inside the γ-CD"), the probabilities of finding one (P_1) or two (P_2) azlocillin molecules inside the γ-CD are $P_1 = 0.53 \times 10^{-4}$ and $P_2 = 1.45 \times 10^{-9}$, respectively. What these numbers tell us is that, although in theory there is a very slim chance of capturing simultaneously two azlocillin molecules inside the γ-CD, the collective experimental manifestation of electrophoretic and electro-osmotic driving forces on azlocillin renders such capture events more likely.

Furthermore, the influence of the ionization state of the trans-added azlocillin on translocation across γ-CD was assessed by comparative Fourier analysis on the ionic current fluctuations ($\Delta I_{azlocillin/\gamma\text{-CD}}$) recorded under symmetric neutral pH conditions (pH trans = 7.1, pH cis = 7.1) (Figure 4b) versus oppositely oriented, asymmetric pH changes (pH trans ∼ 3, pH cis = 7.1; Figure 4c and pH trans = 7.1, pH cis ∼ 3; Figure 4d, respectively). In doing so, we sought to (i) meet the need for probing azlocillin-γ-CD interactions at longer time scales due to the low pH-induced, γ-CD stabilization inside the nanopore, and (ii) retain the opportunity of comparing azlocillin-γ-CD interactions at distinct ionization states of azlocillin, as set by the trans pH value, yet under roughly similar conditions from the perspective of electro-osmotic flow action.

As concluded from data in Figure 4e, the corner frequency (f_c), defined herein as the frequency where the relative PSD value decreases to 0.5, of the power spectrum density spectra changes from $f_c = 92.2 \pm 14$ Hz (mean ± SEM; pH trans = 7.1,

https://doi.org/10.1021/acs.analchem.4c06801
Anal. Chem. 2025, 97, 5225−5233

pH cis = 7.1) to f_c = 34.5 ± 6.1 Hz (mean ± SEM; pH trans ∼ 3, pH cis = 7.1) and f_c = 45.7 ± 4.8 Hz (mean ± SEM; pH trans = 7.1, pH cis ∼ 3), respectively. Control experiments (Figures S10 and S11) demonstrate that the kinetic changes revealed in Figure 4b,c do not reflect pH-induced modifications of the intrinsic current fluctuation events associated with the dynamics of a captured γ-CD molecule inside the α-HL. Data above suggest that altering the ionization state of azlocillin through lowering the trans side pH leads to the formation of more stable azlocillin-γ-CD complexes, qualitatively similar to previous reports.[64] At this point, the question lingers as to whether the electro-osmotic flow manifested in such conditions (pH ∼ 3 trans; pH = 7.1 cis) contributes to the seen kinetics describing the azlocillin-γ-CD interactions (*vide supra*). To address this, it is worth noting that under asymmetrical acidic pH changes, it is expected not to alter the net charge on the trans-added azlocillin and still preserve the elo direction (pH = 7 trans; pH ∼ 3 cis, Figure 4d); the overall kinetic underlying $\Delta I_{azlocillin/\gamma\text{-CD}}$ fluctuations resemble data recorded at neutral pH (Figure 4b). This is evidence that the slower kinetic describing azlocillin-γ-CD interactions in Figure 4c (pH ∼ 3 trans; pH = 7.1 cis) is determined chiefly by the low pH-generated, reduced azlocillin charge. However, in the latter case (Figure 4d), the kinetic recovery remains slower than that recorded under symmetrical, neutral pH (Figure 4b,e). Whether this reflects the dynamic change of azlocillin protonation inside the α-HL's β-barrel due to the existing local $[H]^+$ gradient (Figure S12), it yet remains to be established.

CONCLUSIONS

Drawing on the size compatibility of cyclodextrins with α-HL, we explored herein the host−guest interactions of selected 5-mers homonucleotides, termed A5 and T5, with a γ-CD captured within the α-HL nanopore. We found that the "molecular fingerprint" that permits single-molecule identification of A5 and T5 fragments inside the γ-CD-α-HL complex depends on the capture side of the γ-CD. We also show that an asymmetric, low pH-mediated electro-osmotic flow has a profound impact on stabilizing a γ-CD inside α-HL, circumventing the need for covalently attaching the adapter inside the pore. Contrastingly, we found that the reversible host (γ-CD)−guest (analyte) interactions are hardly affected by the electro-osmotic flow. Our data also reveal that the orientation of the electro-osmotic flow via the control on the applied ΔV constitutes an effective tool to achieve pulling it in and out of the nanopore of a γ-CD, and it provides a simple solution to programmable detection of analytes with the γ-CD-α-HL. The presented findings are in full accord with previous ones, illustrating the manifestation of electro-osmotic flow as a dominant driving force acting on neutral cyclodextrins or other nonionic polymers, rendered without the chemical modifications of the nanopore.[43,65,66] The possibility of lengthening the residence time of γ-CD inside the α-HL with a controlled pH asymmetry, to enable better statistics on stochastic guest (analyte)−γ-CD (host) interactions, enabled the more efficient visualization of azlocillin blockade events and revealed its pH-dependent interaction with the inner volume γ-CD at the single-molecule level.

ASSOCIATED CONTENT

Supporting Information

The Supporting Information is available free of charge at https://pubs.acs.org/doi/10.1021/acs.analchem.4c06801.

Additional experimental details, data, and statistics regarding the α-H-γ-CD-ssDNA interactions (PDF)

AUTHOR INFORMATION

Corresponding Authors

Yoonkyung Park − *Department of Biomedical Science and Research Center for Proteinaceous Materials (RCPM), Chosun University, 61452 Gwangju, Republic of Korea;* orcid.org/0000-0002-8717-3080; Email: y_k_park@chosun.ac.kr

Tudor Luchian − *Department of Physics, Alexandru I. Cuza University, 700506 Iasi, Romania;* orcid.org/0000-0002-9388-7266; Email: luchian@uaic.ro

Authors

Loredana Mereuta − *Department of Physics, Alexandru I. Cuza University, 700506 Iasi, Romania*

Adina Cimpanu − *Department of Physics, Alexandru I. Cuza University, 700506 Iasi, Romania*

Jonggwan Park − *Department of Bioinformatics, Kongju National University, 32588 Kongju, Republic of Korea*

Complete contact information is available at: https://pubs.acs.org/10.1021/acs.analchem.4c06801

Author Contributions

#L.M., A.C., and J.P. contributed equally to this paper. The manuscript was written through contributions of all authors. All authors have given approval to the final version of the manuscript.

Notes

The authors declare no competing financial interest.

ACKNOWLEDGMENTS

This work was supported by the National Research Foundation of Korea (NRF; Grant Numbers 2023R1A2C3006368, RS-2023-00228746, RS-2024-00401422, and RS-2023-00253613), the Institute for Information and Communications Technology Promotion (IITP) Grant from the Korean government (MSIT; Grant Number RS-2017-II171714, Development of Antimicrobial Peptide using Deep Learning), and UEFISCDI Grant PN-IV-P1-PCE-2023-0678 (Romania).

REFERENCES

(1) Kasianowicz, J. J.; Robertson, J. W. F.; Chan, E. R.; Reiner, J. E.; Stanford, V. M. *Annual Rev. Anal. Chem.* **2008**, *1*, 737−766.

(2) Howorka, S.; Siwy, Z. *Chem. Soc. Rev.* **2009**, *38*, 2360.

(3) Luchian, T.; Shin, S.; Bayley, H. *Angew. Chem. Int. Ed.* **2003**, *42*, 1926−1929.

(4) Tanimoto, I. M. F.; Cressiot, B.; Greive, S. J.; Le Pioufle, B.; Bacri, L.; Pelta, J. *Nano Res.* **2022**, *15*, 9906−9920.

(5) Kasianowicz, J. J.; Brandin, E.; Branton, D.; Deamer, D. W. *Proc. Natl. Acad. Sci. U.S.A.* **1996**, *93*, 13770−13773.

(6) Laszlo, A. H.; Derrington, I. M.; Ross, B. C.; Brinkerhoff, H.; Adey, A.; Nova, I. C.; Craig, J. M.; Langford, K. W.; Samson, J. M.; Daza, R.; Doering, K.; Shendure, J.; Gundlach, J. H. *Nat. Biotechnol.* **2014**, *32*, 829−833.

(7) Cao, C.; Ying, Y.-L.; Hu, Z.-L.; Liao, D.-F.; Tian, H.; Long, Y.-T. *Nat. Nanotechnol.* **2016**, *11*, 713−718.

(8) Clarke, J.; Wu, H.-C.; Jayasinghe, L.; Patel, A.; Reid, S.; Bayley, H. *Nat. Nanotechnol.* **2009**, *4*, 265−270.
(9) Song, L.; Hobaugh, M. R.; Shustak, C.; Cheley, S.; Bayley, H.; Gouaux, J. E. *Science* **1996**, *274*, 1859−1865.
(10) Derrington, I. M.; Butler, T. Z.; Collins, M. D.; Manrao, E.; Pavlenok, M.; Niederweis, M.; Gundlach, J. H. *Proc. Natl. Acad. Sci. U.S.A.* **2010**, *107*, 16060−16065.
(11) Cao, C.; Li, M.-Y.; Cirauqui, N.; Wang, Y.-Q.; Dal Peraro, M.; Tian, H.; Long, Y.-T. *Nat. Commun.* **2018**, *9*, 2823.
(12) Mayer, S. F.; Cao, C.; Dal Peraro, M. *Biological Nanopores for Single-Molecule Sensing. iScience* **2022**, *25*, 104145.
(13) Tanaka, K.; Caaveiro, J. M. M.; Morante, K.; González-Mañas, J. M.; Tsumoto, K. *Nat. Commun.* **2015**, *6*, 6337.
(14) Van Der Verren, S. E.; Van Gerven, N.; Jonckheere, W.; Hambley, R.; Singh, P.; Kilgour, J.; Jordan, M.; Wallace, E. J.; Jayasinghe, L.; Remaut, H. *Nat. Biotechnol.* **2020**, *38*, 1415−1420.
(15) Alfaro, J. A.; Bohländer, P.; Dai, M.; Filius, M.; Howard, C. J.; Van Kooten, X. F.; Ohayon, S.; Pomorski, A.; Schmid, S.; Aksimentiev, A.; Anslyn, E. V.; Bedran, G.; Cao, C.; Chinappi, M.; Coyaud, E.; Dekker, C.; Dittmar, G.; Drachman, N.; Eelkema, R.; Goodlett, D.; Hentz, S.; Kalathiya, U.; Kelleher, N. L.; Kelly, R. T.; Kelman, Z.; Kim, S. H.; Kuster, B.; Rodriguez-Larrea, D.; Lindsay, S.; Maglia, G.; Marcotte, E. M.; Marino, J. P.; Masselon, C.; Mayer, M.; Samaras, P.; Sarthak, K.; Sepiashvili, L.; Stein, D.; Wanunu, M.; Wilhelm, M.; Yin, P.; Meller, A.; Joo, C. *Nat. Methods.* **2021**, *18*, 604−617.
(16) Kennedy, E.; Dong, Z.; Tennant, C.; Timp, G. *Nat. Nanotechnol.* **2016**, *11*, 968−976.
(17) Ouldali, H.; Sarthak, K.; Ensslen, T.; Piguet, F.; Manivet, P.; Pelta, J.; Behrends, J. C.; Aksimentiev, A.; Oukhaled, A. *Nat. Biotechnol.* **2020**, *38*, 176−181.
(18) Piguet, F.; Ouldali, H.; Pastoriza-Gallego, M.; Manivet, P.; Pelta, J.; Oukhaled, A. *Nat. Commun.* **2018**, *9*, 966.
(19) Luchian, T.; Park, Y.; Asandei, A.; Schiopu, I.; Mereuta, L.; Apetrei, A. *Acc. Chem. Res.* **2019**, *52*, 267−276.
(20) Afshar Bakshloo, M.; Kasianowicz, J. J.; Pastoriza-Gallego, M.; Mathé, J.; Daniel, R.; Piguet, F.; Oukhaled, A. *J. Am. Chem. Soc.* **2022**, *144*, 2716−2725.
(21) Bayat, P.; Rambaud, C.; Priem, B.; Bourderioux, M.; Bilong, M.; Poyer, S.; Pastoriza-Gallego, M.; Oukhaled, A.; Mathé, J.; Daniel, R. *Nat. Commun.* **2022**, *13*, 5113.
(22) Keyser, U. F.; Koeleman, B. N.; Van Dorp, S.; Krapf, D.; Smeets, R. M. M.; Lemay, S. G.; Dekker, N. H.; Dekker, C. *Nat. Phys.* **2006**, *2*, 473−477.
(23) Mereuta, L.; Asandei, A.; Dragomir, I.; Park, J.; Park, Y.; Luchian, T. *Anal. Chem.* **2022**, *94*, 8774−8782.
(24) McCord, B. R.; Gauthier, Q.; Cho, S.; Roig, M. N.; Gibson-Daw, G. C.; Young, B.; Taglia, F.; Zapico, S. C.; Mariot, R. F.; Lee, S. B.; Duncan, G. *Anal. Chem.* **2019**, *91*, 673−688.
(25) Li, M.; Yin, F.; Song, L.; Mao, X.; Li, F.; Fan, C.; Zuo, X.; Xia, Q. *Chem. Rev.* **2021**, *121*, 10469−10558.
(26) Boutonnet, A.; Pradines, A.; Mano, M.; Kreczman-Brun, M.; Mazières, J.; Favre, G.; Ginot, F. *Anal. Chem.* **2023**, *95*, 9263−9270.
(27) Davenport, M.; Healy, K.; Pevarnik, M.; Teslich, N.; Cabrini, S.; Morrison, A. P.; Siwy, Z. S.; Létant, S. E. *ACS Nano* **2012**, *6*, 8366−8380.
(28) Rincon-Restrepo, M.; Mikhailova, E.; Bayley, H.; Maglia, G. *Nano Lett.* **2011**, *11*, 746−750.
(29) Maglia, G.; Restrepo, M. R.; Mikhailova, E.; Bayley, H. *Proc. Natl. Acad. Sci. U.S.A.* **2008**, *105*, 19720−19725.
(30) Mereuta, L.; Bhatti, H.; Asandei, A.; Cimpanu, A.; Ying, Y.-L.; Long, Y.-T.; Luchian, T. *ACS Appl. Mater. Interfaces* **2024**, *16*, 40100−40110.
(31) Fologea, D.; Uplinger, J.; Thomas, B.; McNabb, D. S.; Li, J. *Nano Lett.* **2005**, *5*, 1734−1737.
(32) Nova, I. C.; Derrington, I. M.; Craig, J. M.; Noakes, M. T.; Tickman, B. I.; Doering, K.; Higinbotham, H.; Laszlo, A. H.; Gundlach, J. H. *PLoS One* **2017**, *12*, No. e0181599.
(33) De Zoysa, R. S. S.; Krishantha, D. M. M.; Zhao, Q.; Gupta, J.; Guan, X. *Electrophoresis* **2011**, *32*, 3034−3041.
(34) Mereuta, L.; Asandei, A.; Andricioaei, I.; Park, J.; Park, Y.; Luchian, T. *Nanoscale* **2023**, *15*, 14754−14763.
(35) Anderson, B. N.; Muthukumar, M.; Meller, A. *ACS Nano* **2013**, *7*, 1408−1414.
(36) Payet, L.; Martinho, M.; Merstorf, C.; Pastoriza-Gallego, M.; Pelta, J.; Viasnoff, V.; Auvray, L.; Muthukumar, M.; Mathé, J. *Biophys. J.* **2015**, *109*, 1600−1607.
(37) Huang, G.; Willems, K.; Bartelds, M.; Van Dorpe, P.; Soskine, M.; Maglia, G. *Nano Lett.* **2020**, *20*, 3819−3827.
(38) Wong, C. T. A.; Muthukumar, M. *J. Chem. Phys.* **2007**, *126*, 164903.
(39) Schmid, S.; Stömmer, P.; Dietz, H.; Dekker, C. *Nat. Nanotechnol.* **2021**, *16*, 1244−1250.
(40) Gubbiotti, A.; Baldelli, M.; Di Muccio, G.; Malgaretti, P.; Marbach, S.; Chinappi, M. *Adv. Phys.: X* **2022**, *7*, 2036638.
(41) Huang, G.; Willems, K.; Soskine, M.; Wloka, C.; Maglia, G. *Nat. Commun.* **2017**, *8*, 935.
(42) Asandei, A.; Schiopu, I.; Chinappi, M.; Seo, C. H.; Park, Y.; Luchian, T. *ACS Appl. Mater. Interfaces* **2016**, *8*, 13166−13179.
(43) Gu, L.-Q.; Cheley, S.; Bayley, H. *Proc. Natl. Acad. Sci. U.S.A.* **2003**, *100*, 15498−15503.
(44) Firnkes, M.; Pedone, D.; Knezevic, J.; Döblinger, M.; Rant, U. *Nano Lett.* **2010**, *10*, 2162−2167.
(45) Bafna, J. A.; Pangeni, S.; Winterhalter, M.; Aksoyoglu, M. A. *Biophys. J.* **2020**, *118*, 2844−2852.
(46) Soni, N.; Chandra Verma, N.; Talor, N.; Meller, A. *Nano Lett.* **2023**, *23*, 4609−4616.
(47) Mereuta, L.; Roy, M.; Asandei, A.; Lee, J. K.; Park, Y.; Andricioaei, I.; Luchian, T. *Sci. Rep.* **2014**, *4*, 3885.
(48) Li, M.; Muthukumar, M. *J. Chem. Phys.* **2024**, *160*, No. 084905.
(49) Gu, L.-Q.; Braha, O.; Conlan, S.; Cheley, S.; Bayley, H. *Nature* **1999**, *398*, 686−690.
(50) Gu, L.-Q.; Bayley, H. *Biophys. J.* **2000**, *79*, 1967−1975.
(51) Astier, Y.; Braha, O.; Bayley, H. *J. Am. Chem. Soc.* **2006**, *128*, 1705−1710.
(52) Asandei, A.; Mereuta, L.; Luchian, T. *J. Phys. Chem. B* **2011**, *115*, 10173−10181.
(53) Gu, L.-Q.; Dalla Serra, M.; Vincent, J. B.; Vigh, G.; Cheley, S.; Braha, O.; Bayley, H. *Proc. Natl. Acad. Sci. U.S.A.* **2000**, *97*, 3959−3964.
(54) Wei, X.; Choudhary, A.; Wang, L. Y.; Yang, L.; Uline, M. J.; Tagliazucchi, M.; Wang, Q.; Bedrov, D.; Liu, C. *Sci. Adv.* **2024**, *10*, No. eadp8134.
(55) Sanchez-Quesada, J.; Ghadiri, M. R.; Bayley, H.; Braha, O. *J. Am. Chem. Soc.* **2000**, *122*, 11757−11766.
(56) Braha, O.; Webb, J.; Gu, L.; Kim, K.; Bayley, H. *ChemPhysChem* **2005**, *6*, 889−892.
(57) Van De Manakker, F.; Vermonden, T.; Van Nostrum, C. F.; Hennink, W. E. *Biomacromolecules* **2009**, *10*, 3157−3175.
(58) Kowalczyk, S. W.; Grosberg, A. Y.; Rabin, Y.; Dekker, C. *Nanotechnology* **2011**, *22*, 315101.
(59) Nadassy, K.; Tomás-Oliveira, I.; Alberts, I.; Janin, J.; J, S. J. *Nucleic Acids Res.* **2001**, *29*, 3362−3376.
(60) Gu, L.-Q.; Cheley, S.; Bayley, H. *J. Gen. Physiol.* **2001**, *118*, 481−494.
(61) Boczar, D.; Michalska, K. *Pharmaceutics* **2022**, *14*, 1389.
(62) Samuelsen, L.; Holm, R.; Schönbeck, C. *J. Drug Delivery Sci. Technol.* **2021**, *65*, 102675.
(63) PubChem Compound Summary for CID 6479523, Azlocillin. https://pubchem.ncbi.nlm.nih.gov/compound/Azlocillin (accessed 2024−11−24).
(64) Aki, H.; Ikeda, H.; Yukawa, M.; Iwase, Y.; Mibu, N. *J. Therm. Anal. Calorim.* **2009**, *95*, 421−426.
(65) Boukhet, M.; Piguet, F.; Ouldali, H.; Pastoriza-Gallego, M.; Pelta, J.; Oukhaled, A. *Nanoscale* **2016**, *8*, 18352−18359.
(66) Piguet, F.; Discala, F.; Breton, M.-F.; Pelta, J.; Bacri, L.; Oukhaled, A. *J. Phys. Chem. Lett.* **2014**, *5* (24), 4362−4367.

https://doi.org/10.1021/acs.analchem.4c06801
Anal. Chem. 2025, 97, 5225−5233